Journal of Pioneering Medical Sciences
Received: September 24, 2025 | Accepted: February 15, 2026 | Published: April 05, 2026
Volume 15, Issue 03, Pages 179-188

DOI https://doi.org/10.47310/jpms2026150328

The Effect of Magnesium Nanoparticles MgNPs and Some Antibiotics on the Escherichia coli Isolated from Different Infections

Abdul Sattar Abdul Jabbar Ibrahim[1], Mahnoud Shukor Mughir[2] and Adawia Fadhil Abbas Alzubaidi[3*]
[1,2]Diyala Education Directorate, Ministry of Education, Diyala, Iraq
[3]Department of Biology, College of Education for Pure Science, Diyala University, Iraq

*Corresponding author: Adawia Fadhil Abbas Alzubaidi (e-mail: Adawiaalzubaidi.2015@gmail.com).

Abstract Because bacteria are resistant to medications, their capacity to create biofilms has made the healing process of infections more difficult. Thus, the current study sought to identify a different approach of employing nanotechnology to inhibit bacteria. The biological activity of bacteria against multidrug-resistant *Escherichia coli* isolated from a variety of diseases in the Diyala Governorate was investigated using magnesium nanoparticles (MgNPs) in conjunction with particular antibiotics. 155 samples were taken from patients with a variety of inflammatory diseases who were admitted to Baqubah Teaching Hospital between August 2024 and January 2025. Microscopy, morphological analysis and VITEC technology were used to characterize the isolates. The susceptibility to antibiotics was tested using the Kirby-Bauer disk diffusion method. The findings demonstrated that 58 *E. coli* isolate samples shown resistance to widely used antibiotics. Antibiotics and magnesium nanoparticles were used as treatments to evaluate the isolates. The findings demonstrated that as magnesium nanoparticle concentration increased, the *E. coli* inhibition zone progressively expanded, attaining optimal inhibition at 400 µg/ml and 0.01 mg/ml, respectively. Congo red agar was one of the phenotypic methods used to assess the capacity of particular *E. coli* isolates to produce biofilms. **Methods:** Ten (17.2%) of the 58 (100%) *E. coli* isolates did not form biofilms when the colonies remained pink or red, while 48 (82.8%) did so when dark, dry and crystalline colonies formed on CRA plates. The *E. coli* isolates were found to have the antibiotic resistance genes gyrA, Sul1, Ant (2)-1a, ermB, blaSHV and qnrA by molecular analysis. The goal of this research is to develop novel therapeutic medicines to manage specific illnesses and slow the spread of bacteria resistant to antibiotics.

Key Words *E. coli*, Antibacterial Activity, Magnesium Nanoparticles

INTRODUCTION

The use of antibiotics has significantly influenced the growth of multidrug-resistant bacteria, which can cause infections and lead to chronic or persistent infections [1]. Biofilms, a collection of cells on a surface encased in an exterior polymer matrix, can limit material diffusion and antimicrobial binding, protecting biofilm cells against antibacterial proteins like complement and lysozyme. Chronic infections are believed to be caused by bacteria's ability to build biofilms, which aid in their survival in the host's hostile environment [2].

Biofilms play a role in human illnesses and breaking through these biofilms is considered a harmful characteristic in contemporary clinical microbiology [3]. Magnesium nanotechnology can potentially stop potentially fatal biofilms from growing on medical equipment. *E. coli* strains, found in the bottom portion of the small intestine, can cause gastroenteritis, Crohn's disease, septic shock, hemorrhagic colitis and newborn meningitis. Bloody diarrhea, a sign of Shiga toxin *E. coli* (STEC), can result from lesions caused by one of these strains, O157:H7 [4]. Hemolytic Uremic Syndrome (HUS), which can result in kidney failure and even death, is brought on by Shiga toxin, which produces inflammatory responses in certain intestinal cells [5,6].

Antibiotic therapy is a common treatment for *E. coli* infections but isolates resistant to multiple antibiotics are a global public health concern. Antibiotics often work well

against bacteria but they need higher dosages to have an impact when the microorganisms grow less sensitive or resistant [7]. When a medication loses its capacity to efficiently stop bacterial growth, antibiotic resistance develops. Several Enterobacteriaceae strains are naturally resistant to a number of antibiotic families due to the presence of a second molecule known as OM [8,9]. Magnesium is used worldwide as a dietary supplement, food color stabilizer, pH regulator and in various products, including fertilizers, antacids, laxatives, PVCs and resins [10]. Magnesium nanoparticles are used in antibacterial materials, biomaterials for minimally inflammatory implants and glaucoma treatment. Recent research on antimicrobial nanoparticles has focused on their high sterilizing capacity, safety and usefulness [11,12].

METHODS

Collection of Samples

The total number of clinical samples collected between August 2024 and January 2025 was 155. Urine exchanges and clinical samples were collected from Iraqi patients in the Diyala hospitals (Ba'aqubah Teaching Hospital, Al-Batool Teaching Hospital) in Ba'aqubah.

Bacterial Isolation and Identification

By growing the collected clinical samples on selective and differential media, *Escherichia coli* was recovered. Clinical samples were immediately inoculated on both blood agar and MacConkey agar and then incubated for 24 hours at 37°C. Afterwards, the former colonies were further examined using biochemical assays and the Vitek system. Magnesium nanoparticle preparation, per Pavel *et al.*

Antibiotic Susceptibility Testing

To ascertain their susceptibility to 16 distinct antibiotics, all 58 clinical *Escherichia coli* isolates (37.3%) underwent an antibiotic sensitivity test using the Kirby-Bauer method: 30 mg of Cefazolin (KZ), 30 mg of Cefoxitin (FX), 30 mg of Ceftazidime (CRO), 30 mg of Cefepime (FEP), 10 mg of Ertapenem (ETP), 10 mg of Imipenem (IPM), 30 mg of Amikacin (AK), 10 mg of Gentamicin (GM), 5 mg of Ciprofloxacin (CIP), 5 mg of Levofloxacin (LVX), 15 mg of Tigecycline (TGC), 300 mg of Nitrofurantoin (F) and 25 mg of Trimethoprim (SXT). The antibiotic discs used in the procedure was created using the disc diffusion method in compliance with the guidelines made by the National Committee for Clinical Laboratory Standards (2024) and it was confirmed by the VITEK2 compact system.

Antibacterial Activity of Magnesium Nanoparticles (MgNPs) Against MDR *E. coli* Isolated Growth

To check for antibiotic resistance, Muller Hinton Agar is prepared by autoclaving it and then transferring it into petri dishes. E was streaked using a sterile swab. On a petri plate, Coli isolates. The antibacterial activity of the magnesium nanoparticles at four concentrations (100, 200, 300 and 400 µg/ml) was assessed using the agar well diffusion assay method. Following a 24 hour incubation period at 37°C, the plates were examined for indications of an inhibition zone-a transparent region encircling the wells. A meter ruler was used to measure the inhibitory zones' diameter [6].

Detection of Biofilm Production

Congo red agar was used to test for the production of biofilms by clinical isolates of *E. coli*. The capacity of the bacteria to form the slime layer was assessed using this medium. When black colonies with a dry, crystalline quality were present, the isolates were regarded as strongly positive. In order to make Congo red agar, 37 grams of brain heart infusion broth, 50 grams of sucrose and 15 grams of agar-agar were dissolved in 900 millilitres of distilled water. The mixture was then autoclaved, cooled to 55 to 60 degrees Celsius and then Congo red solution-which was created by dissolving 0.8 grams of Congo red dye in 100 millilitres of distilled water and sterilising it by filtering-was added. Sterile Petri dishes were filled with the prepared medium.

Prepare Magnesium Nanoparticles (MgNPs)

The actual density of MgNPs is 3.57 g/cm3. Since MgNPs cannot be sterilised or disinfected by conventional means, they were sterilised for this investigation by heating them in an oven at 190°C for an hour before each in vitro experiment. Given that MgNPs are hygroscopic, autoclaving is not the best sterilising technique because the water in the steam alters the phase, which compromises the precision of test findings against microbes. Moreover, UV should not be utilised to disinfect MgNPs since they absorb UV light and interact with oxygen molecules. SEM microscopy was used to characterise the nanoparticles. Using energy dispersive X-ray spectroscopy and X-ray diffraction, respectively, to ascertain the zeta potential of MgNPs, the phase and elemental composition of these nanoparticles were verified. The diluent, water, had a dielectric constant of 77.3, a viscosity of 0.88 cP and a refractive index of 1.30. An applied voltage of 5 V/cm and room temperature of 26°C were used for the test. The zeta potential of MgO was computed using the Huckel equation and the electrical mobility of MgNPs was determined using the Laser Doppler method based on the frequency shift of the scattered light [13,14].

Characterisation of MgNPs

The characterisation of the biosynthesized MgNPs was applied according to Darwich *et al.* as follows:

- **X-Ray Diffraction (XRD):** XRD was used to determine the MgNPs' crystalline structure. The XRD patterns were examined using a Bruker D8 Advance (Bruker, Ettlingen, Germany) fitted with Cu-Kα radiation at a wavelength of 1.54060 A. The data were

gathered at a rate of 0.02° per second throughout a 2θ range of 20-80°. The MAUD program (version 2.992) was used to improve the XRD profiles

- **Transmission Electron Microscopy (TEM):** TEM was used to determine the MgNPs' average particle size. A transmission electron microscope (JEOL, Tokyo, Japan) running at 80 kV and 0.1 nm resolution was used for the test. The 100 nm magnification TEM images were analysed using ImageJ software (version 1.54 g)
- **Fourier Transform Infrared Spectroscopy (FTIR):** A Fourier transform infrared spectrophotometer (FTIR-8400S, Nicolet iS5, ThermoScientific, Berlin, Germany) operating in the 4000-500 cm^{-1} spectral range was used to identify the functional groups of the MgNPs at ambient temperature.
- **Photoluminescence (PL):** The PL spectra were obtained using a Xenon (Xe) laser and a fluorescence spectrophotometer (JASCO-FP-8600, JASCO, Pfungstadt, Germany) at an excitation wavelength of 420 nm and within the 200-700 nm range
- **Ultraviolet-Visible Spectroscopy (UV-Vis):** A UV-Vis spectrophotometer (V-670; Jasco, Tokyo, Japan) was used to evaluate the optical properties of the MgNPs at room temperature and within a 270-280 nm range

Biofilm Formation Assays

The capacity of the biosynthesised MgNPs and BMs to prevent the formation of bacterial biofilms was tested using the inhibition of biofilm formation assay. 90 µL of MHB was added to 10 µL of the prepared bacterial suspensions in 96-well microtiter plates to conduct the test. To enable the biofilms to adhere, the plates were cultured for three hours at 37°C. Following incubation, the wells were filled with 100 µL of the produced MgNPs at concentrations ranging from 0.03125 to 4 mg/mL (beginning at MIC×2) and BMs (at 100% concentration). Once more, the plates were incubated for 24 hours at 37°C. As a control, cultures that received no treatment were employed. Following incubation, the plates were dried in an oven set to 40°C for 15 minutes and rinsed three times with sterile distilled water. The wells were stained with 1% crystal violet (CV; Alpha Chemika, CV506, Mumbai, India) and allowed to sit at room temperature for 15 minutes in order to see the biofilms. The biofilms were then seen as purple rings on the well walls after the plates had been cleaned five times with sterile distilled water. After de-staining the wells with 100 µL of 100% ethanol (200/190, HAKINMHAN), the biofilms were quantified by measuring the O.D. at 595 nm with an ELISA reader [15]. The following Equation 1 was used to quantify the biofilms:

$$\text{Percentage of biofilm inhibition } (\%) = \frac{\text{O.D. (negative contro) O.D.(treated sample)}}{\text{O.D. (negative control)}} \times 100 \quad (1)$$

To find out if the biosynthesized MgNPs and BMs could destroy pre-formed biofilms, a similar procedure to the inhibition of biofilm formation was used. The sole distinction was that the bacteria were incubated in MHB for 30 hours in order to develop biofilms prior to treatment. The methods used for staining and quantifying were the same as those used to suppress the formation of biofilms [16].

Anti-Biofilm Activity of MgNPs. against MDR *E. coli* Isolated Growth

CRA plates were inoculated with isolated *E. coli* using a specially prepared medium known as Congo red agar. The plates were then grown aerobically for 48 hours at 37°C. The presence of black dry crystalline colonies suggested the generation of biofilm, whereas the colonies of biofilm nonproducers remained pink or red in color. Following the streaking of a colony of biofilm-forming *E. coli* isolates on CRA plates, a sterile cork porer was used to inject four different concentrations of magnesium (100, 200, 300 and 400 µg/ml). Inhibitory zone diameters were evaluated after a 24 hour incubation period at 37°C.

Statistical Analysis

Every experiment was conducted three times to guarantee statistical confidence. The mean ± standard error of the mean was used to record the experimental results. The significance was assessed using a t-test and a p-value of less than 0.05 was deemed statistically significant. Excel software (64-bit edition) was used to conduct statistical significance tests (t-tests) and Origin program (64-bit version) was used to create graphics.

RESULTS AND DISCUSSION

Identification of the Clinical Bacteria Strains

VITEK was used to identify the bacterial isolates. A quick method for identifying microorganisms, particularly bacteria, is the VITEK assay. 155 bacterial isolates are identified using a variety of biochemical tests. The following are the VITEK results for the bacterial isolates: Gram-negative bacteria included *E. coli* 58 (374%), *K. pneumonia* 32 (20.6%) and *S. typhimurium* 15 (9.7%), whereas Gram-positive bacteria included *S. pneumonia* 23 (14.8%) and *E. fecium* 27 (17.4%). Excellent (96-99%), very good (93-95%), good (89-92%) and acceptable (85-88%) were the classifications given to the identification levels [17]. Table 1 displays the findings and the degrees of identification.

Table 1: Identification of the Clinical Bacterial Isolates

Bacterial isolates	No. (%)
E. coli	58(37.4%)
S. pneumonia	23(14.8%)
E. faecium	27(17.4%)
K. pneumonia	32(20.6%)
S. typhimurium	15 (9.7%)
Total	155 (100%)

Characterization

X-Ray Diffraction (XRD): One method for determining the crystalline structure of NPs is XRD It is predicated on the measurement of different atomic configurations and structural characteristics of the crystalline phases. The XRD patterns of the MgNPs are shown in Figure 1, where six diffraction peaks are visible. Peaks at 27.2°, 32.8°, 38.6°, 46.9°, 64.9° and 78.5° were noted. There has never been a peak at 27.2° (202) in NPs produced by bacteria. It probably relates to a little crystalline impurity that developed during the drying process. The strong reactivity of the MgNPs may be the cause of this interpretation. Furthermore, the existence of some contaminants as a result of the capping agents used during the synthesis process may possibly account for the minor peaks seen [18].

On the other hand, the maxima at 32.8°, 38.6°, 46.9°, 64.9° and 78.5°, respectively, reflect (111), (200), (220), (311) and (222). These peaks show the cubic phase of magnesium and validate the crystalline structure of the MgNPs. Prior research has demonstrated that these peaks and the NPs' crystallinity account for their tiny size, which falls between 20 and 27 nm [11]. It is well known that MgNPs are extremely prone to oxidation and their XRD patterns frequently show distinctive Mg-oxide (MgO) peaks. But according to a number of studies, MgNPs can hold onto metallic magnesium [15], which is comparable to our situation in which the BMs served as stabilizing and capping agents in addition to reducing agents, helping to keep metallic magnesium in the NP core. Studies on green synthesis have shown similar results, with stabilizing biomolecules offering some protection against total oxidation [19]. Additionally, consistent with previous results, the distinctive peaks at 38.6° and 64.9° are indexed to metallic Mg.

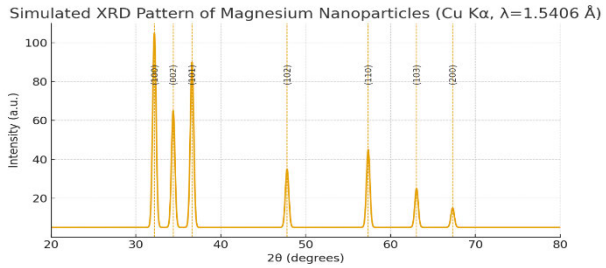

Figure 1: XRD Patterns of the MgNPs Biosynthesized from the Metabolites of *E. coli*

To confirm the size of the biosynthesized MgNPs, the crystalline size was calculated from the XRD data using the Scherrer Equation 3 as follows:

$$D = \frac{K\lambda}{\beta\cos\theta} \quad (3)$$

where, λ is the X-ray wavelength, β is the line broadening at full wide that half maximum (FWHM), θ is the Bragg's angle, D is the average crystalline size and K is Scherrer's constant. Following computations, the average crystalline size of the MgNPs was found to be around 17.41 nm. Additionally, the following Equation 4 was used to determine the degree of crystallinity:

$$\text{Crystallinity} = \frac{\text{Area of crystalline peaks}}{\text{Area of all peaks}} \times 100 \quad (4)$$

The average size of all peaks is 465.39 nm2, while the average area of crystalline peaks is 291.16 nm2. Following computations, the MgNPs' crystallinity percentage came out to be roughly 63.8%. Given the previously reported contaminants in the samples, this finding is compatible with the size of the MgNPs obtained. Our findings are consistent with those of a prior work by Jiang *et al.* which demonstrated that a crystallinity percentage of 60-65% is equivalent to a size of 39-41 nm of NPs [20].

Transmission Electron Microscopy (TEM)

Particle size, shape and distribution can be quantitatively determined with the help of TEM [21]. The MgNPs' TEM micrographs, which are shown in Figure 2b after being annealed at a 100 nm scale, demonstrate that most of the NPs

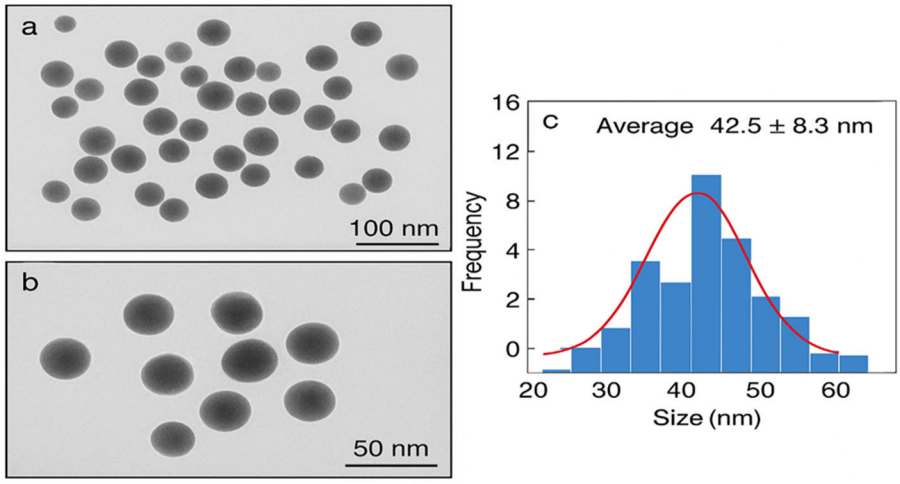

Figure 2: (a) Particle Size Distribution and (b) TEM Images of the MgNPs

are spherical in shape and have a small agglomeration. Furthermore, there is variation in the particle sizes. The capping and reducing agents found in the BMs may be to blame for this. This outcome is comparable to that of Darwich *et al.*, who created yttrium nanoparticles from pine needles and demonstrated agglomeration as a result of the reducing agents in the pine extract they utilized.

The average particle size, as displayed in Figure 2, was roughly 17.8 nm after the particle dimensions were measured using the ImageJ software and the particle size histogram was fitted to the log-normal function [15]. We see that our MgNPs are smaller than those from prior research that focus on MgNPs production. For instance, Amrullah *et al.* [22] demonstrated that MgNPs biosynthesized from Moringa oleifera (*M. oleifera*) extract had particle sizes ranging from 60-100 nm [20]. Furthermore, the production of MgNPs with sizes ranging from 30-100 nm was reported by Abbas *et al.*

The benefit of creating NPs from bacterial metabolites may be explained by this. Additionally, Patil *et al.* demonstrated that plasmonic NPs were larger than 50 nm after synthesizing them from bacterial metabolites [9]. The variations in the BMs and the reactions with the metal nitrate may help to explain this. Our findings were in line with those of a prior study conducted by Hassan *et al.* [23], who produced MgNPs from the fungus R. oryzae and demonstrated a 20 nm particle size [7]. Overall, the MgNPs' TEM data validate their morphology, form and nanosized.

Fourier Transform Infrared Spectroscopy (FTIR)

A useful method for identifying unknown compounds and figuring out the amount and calibre of components in a sample is FTIR [18]. The functional groups contained in the biosynthesised MgNPs were identified using FTIR. Figure 3 shows the results, which show the creation of several vibrational bands. The O-H stretching group is represented by the peaks which are found at 3852.1 and 3429.7 cm^{-1}. The existence of phenolic or alcoholic stretches and several bioactive metabolites explains the O-H group. The N-H stretch is represented by the peak at 3429.7 cm^{-1}. This group explains why the bacterial protein membrane contains amide or amine groups [11].

The existence of alkanes is indicated by the C-H stretching peaks at 2963.3, 2926.4, 2855.2 and 2365.4 cm^{-1} [23]. Furthermore, the peak at 2111.9 might be associated with N=C=S. The C=C, C=O and C=N stretches are represented by the peaks seen at 1739.1, 1649.1 and 1541.1 cm−1, respectively. These account for the existence of aromatic rings in polysaccharides, amides and nucleic acids of the nucleus [24]. The presence of primary amines and aliphatic amino acids is explained by the C-N stretching that corresponds to the peak seen at 1337.9 cm^{-1} [25]. Peaks at 1307.8, 1236.6, 1058.1 and 908.8 cm^{-1} are associated with C-O-H, C-O and C=O stretches, respectively.

The presence of carbonyl groups involved in the conversion of Mg2+ to MgNPs is indicated by these stretches. Furthermore, the presence of C=O indicates

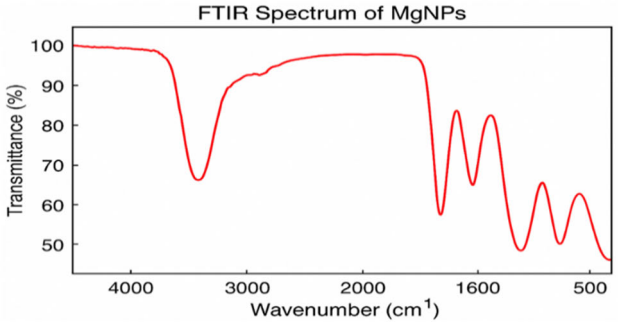

Figure 3: FTIR patterns of the MgNPs biosynthesized from the metabolites of *E. coli*

the existence of carboxylic acid, ester and aldehyde groups [10]. The existence of a connection between the generated MgNPs and OH/CO groups is further supported by the C-O stretching [25]. The functional group of metal bonding (Mg) is responsible for the peaks seen in the 620.3-430.2 cm^{-1} range, indicating Mg stretching [26].

Photoluminescence (PL)

The internal and extrinsic characteristics of the biosynthesized nanostructures were investigated using PL. Using fluorescence emission spectroscopy, the test was conducted at room temperature with an excitation wavelength of 420 nm and within the visible range of 500-4000 nm. The Voigt function deconvoluted the PL spectra. The recombination of electron-hole pairs between the d-band and the sp-conduction area above the Fermi level is what gives the MgNPs their visible luminescence [17].

Defect states in the NPs aid in the electron-hole recombination processes. In particular, the most likely causes are interstitial magnesium deficiencies. Radiative transitions leading to PL are made possible by these intrinsic lattice defects, which produce localised states within the bandgap that serve as recombination centres. By producing donor-like levels in the conduction band, interstitial magnesium deficiencies may also be a factor in emission characteristics. Furthermore, these faulty states may be stabilised or even enhanced by the BMs involved in biosynthesis.

By influencing nucleation and growth, BMs have the ability to adsorb onto the NP surface and may introduce or maintain unsaturated coordination sites and surface vacancies. It has been shown that these biomolecule-NP-NP interactions change the optical behaviour of defects in s NPs [23]. Two peaks were visible in the PL results, which are displayed in Figure 4. At 457.9 nm, a noticeable peak with great intensity was seen. When compared to earlier research, this peak is associated with the blue emission [22].

The blue emission is also associated with the other peak, which was seen at 490.2 nm. Blue emissions have been shown to occur between 454 and 490 nm [6]. The synthesis conditions, NP size and morphology all have an impact on the visible emissions. The recombination of electrons in the Mg vacancies with the hole in the valence band is

responsible for the blue emissions [7]. The excitation of electrons from the d-bands into states above the Fermi level is the process responsible for the visible luminescence. Moreover, an electron from the spp-band recombines with a hole after relaxation via electron-phonon scattering, which results in energy loss and produces photoluminescence through radiative emission [27].

It is important to note that defect-related states, not quantum confinement or doping, are the primary cause of the observed PL in the NPs. The presence of intrinsic defects, such as oxygen vacancies and surface states, which are known to generate luminescence in magnesium nanostructures, is most likely the cause of the PL [9]. Furthermore, the BMs employed in biosynthesis might also influence the behavior of PL. The metabolites have the ability to change the density of surface defects, adsorb onto the NP surface and even add new functional groups that interact with electronic states. PL emission in biosynthesized NPs has been observed to be enhanced or shifted by such surface changes [10].

Ultraviolet-Visible Spectroscopy (UV-Vis)

Using UV-Vis spectroscopy, the chemical characteristics of the MgNPs under test were examined. In the 200-700 nm range, UV-Vis spectroscopy verified the production of MgNPs. Figure 5a displays the UV-Vis data. At 280 nm, the absorption peak was seen. Dolati et colleagues earlier found a similar peak when they produced copper oxide nanoparticles from Bacillus coagulans metabolites. The reduction of magnesium nitrate Mg(NO3)2 to MgNPs is demonstrated by this peak [12].

The surface plasmon resonance commonly reported for metallic MgNPs produced under reducing circumstances is in good agreement with the measured absorption peak [23]. The quantity of colour produced depends on how many electrons are released when NO3 is reduced to NO2. The conversion of Mg2+ to Mg0 is caused by this decrease. Furthermore, metal excitation during MgNPs production is explained by the observed observations [13]. A redox process takes place during the production of MgNPs. In order to create NPs, the Mg2+ ions in Mg (NO3)2 must be converted to metallic Mg (Mg0). NO3 ions participate in this reduction as electron acceptors and undergo partial reduction to NO2.

The degree of reduction, which may be seen visually as a change in the reaction mixture's colour, is determined by the number of electrons that are transferred from the reducing agents (BMs) to NO3. To put it simply, the colour shift shows how many Mg2+ ions have been converted to metallic MgNPs, which shows how far along the reduction reaction is. A single peak's creation previously revealed small-sized NPs, whereas the peak at 270-280 nm suggested a rapid photocatalytic interaction. Because there are no differences in the peaks and absorption intensities, the measured UV data show that the MgNPs are in ideal states [14].

The direct bandgap energy (Eg) of the biosynthesised MgNPs was determined from the absorbance through the relation between the absorption coefficient (α) and the photon energy (hv) according to the following Equation 5 [15]:

$$(\alpha h\nu)\, n = B\,(h\nu - Eg) \quad (5)$$

where, B is a constant and n is an exponent with a value of 2 for the direct transition of the bandgap.

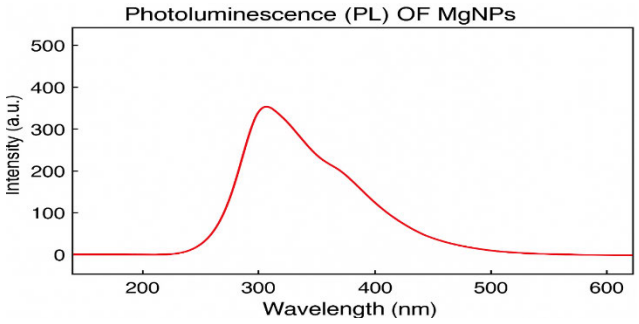

Figure 4: PL Data of the MgNPs Biosynthesized from the Bacterial Metabolites of *E. coli*

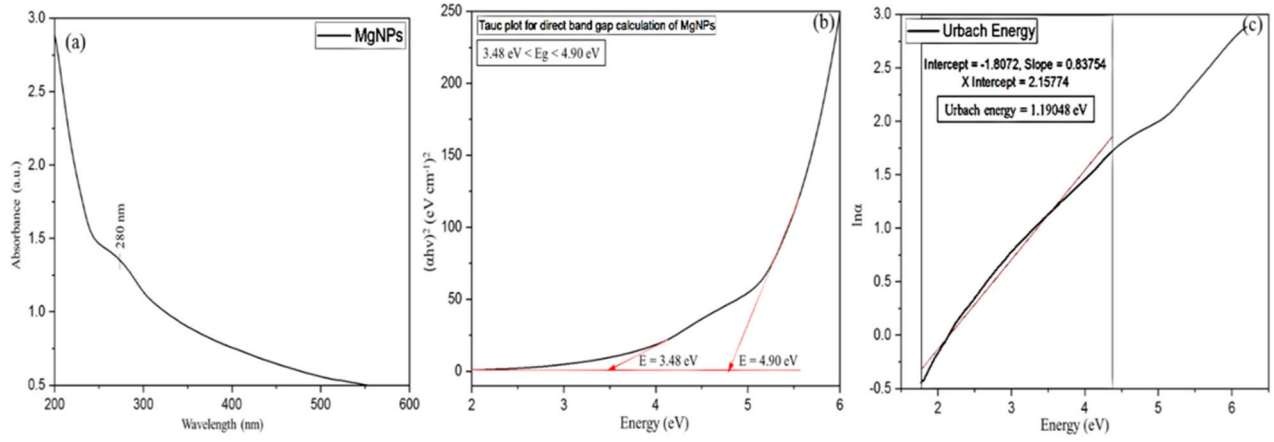

Figure 5: (a) UV-Vis Spectra, (b) Band Gap Energy and (c) Urbach Energy of the MgNPs Biosynthesised from the Metabolites of *E. coli*

The absorption coefficient (α) was calculated using the measured absorbance (A) according to the following Equation 6:

$$\alpha = 2.303\frac{A}{t}$$

Where, t is the path length.

Tauc's Figure (Figure 5b), which extrapolated the linear portion of the (αhν)2 versus photon energy (hν) curve to estimate the bandgap energy, was used to determine the direct bandgap. The average bandgap of the MgNPs was 4.19 eV. This value is consistent with results from previous investigations that used plant-based extracts to synthesise silver nanoparticles. However, the band gap energy was not addressed in any of the earlier publications that reported the synthesis of MgNPs from the BMs. It is well known that overlapping valence and conduction bands are common in bulk metallic magnesium [28].

Because of their decreased dimensionality, high surface-to-volume ratio and surface electrical states, nanoscale materials frequently exhibit characteristics that set them apart from their bulk counterparts. There could be a number of reasons why our NPs show clear band-like characteristics. Localized electronic states and surface plasmon resonance can change the density of states close to the Fermi level at the nanoscale, resulting in transitions that behave like bandgaps. The use of BMs in the biosynthetic process may also lead to surface modification or partial capping, which could introduce extra energy levels or trap states that affect optical absorption and emission.

Lastly, localized states that promote radiative recombination and PL can be produced by inherent flaws or vacancies on the NP surface [18]. Consequently, rather than originating from intrinsic bulk metallic behavior, the unique optical bands and fluorescence seen in our NPs are most likely the consequence of size- and surface-induced phenomena at the nanoscale, as well as defect-related electronic states. The breadth of the localized states' band tails is known as the Urbach energy (Eu). It is computed using Equation (7) [29] and the slope (lnα) of the linear part against photon energy:

$$\alpha = \alpha_0 \exp\frac{hV}{E_u}$$

where, the constant is α0. Figure 5c shows the outcome of the change in lnα as a function of he. The reciprocal of the linear part's slope at the tail area yields the MgNPs' Eu values. 1.19 eV is the obtained Eu value. This is comparable to earlier research that documented how magnesium doping affected copper oxide nanoparticles and magnesium composites.

Antibiotic Susceptibility

Using the disc diffusion method, the antibiotic susceptibility pattern of all 58 (37.3%) *E. coli* isolates that caused different infections in this study was identified to various antibiotics, including piperacillin, ceftazidime, cefazolin and ceftriaxone (ampicillin, cefoxitin, cefepime, ertapenem, imipenem, amikacin, gentamicin, ciprofloxacin, levofloxacin, nitrofurantoin, tigecycline and trimethoprim). This was verified using the VITEK2 system.

According to the findings, all pathogenic *E. coli* isolates exhibited 100% resistance to ampicillin, cefazolin, ceftriaxone, cefepime, trimethoprim and ceftazidime. In contrast, nitrofurantoin, cefoxitin and gentamicin showed 66, 40 and 15% resistance, respectively. As seen in the figure, all isolates were simultaneously susceptible to piperacillin, amikacin, ertapenem, ciprofloxacin, imipenem, levofloxacin and tigecycline (Figure 6).

Antimicrobial resistance studies revealed that *E. coli* isolates were highly resistant to trimethoprim and ampicillin. Vranic and Uzunovic also stated that the study demonstrated that the *E. coli* isolates were highly resistant to cefazolin, ceftriaxone, cefepime and ceftazidime, 100%. That is consistent with the findings of Kader and Kumar as well as Raeis Pour and Ranjbar. According to another study conducted in northern Iraq, *E. coli* isolates showed 100% resistance to cefazolin, ceftriaxone, cefepime, ceftazidime and trimethoprim, whereas 66% resistance to nitrofurantoin [20].

Clinical isolates of *E. coli* produce slime layers. Utilizing the Congo Red Agar technique, the optimal conditions were examined. The findings indicated that 20/58 (34.48%) clinical isolates did not form biofilm, while 38/58 (65.51%) did (Figure 7).

Effect of Different Concentrations of Magnesium Nanoparticles on the Growth of Some MDR Antibiotic Isolates of *E. coli*

The findings showed that as the concentration of magnesium nanoparticles increased, the inhibition zone of resistance in *E. coli* isolates grew larger. At 400 µg/ml, *E. coli* has been shown to have the finest inhibitory zone (26 mm). The electron transport scheme above the plasma membrane is the primary source of ATP in microbes through aerobic respiration. Magnesium ions have the capacity to connect to the specific transporter proteins and enzymes that reside in the microbial plasma membrane. The sequence of proteins and enzymes that carry electrons also concurrently transfers protons from the cytoplasm to the periplasmic area, creating a concentration decline known as the PMF.

The process is also known as chemiosmosis. The only way protons can diffuse back into the cytoplasm is through the ATP formation compound, which contributes to the production of ATP in a redox reaction between ADP and inorganic phosphate. Additionally, when electrons reach the final electron acceptor-melted oxygen in the case of aerobic respiration-they primarily produce water or trace amounts of cytotoxic ROSs, which are produced by particular enzymes [17,22].

Moreover, recent chemical and microbiological studies suggested that the interaction of magnesium ions with thiol groups was crucial for the inactivation of bacteria, despite the widespread belief that heavy metals

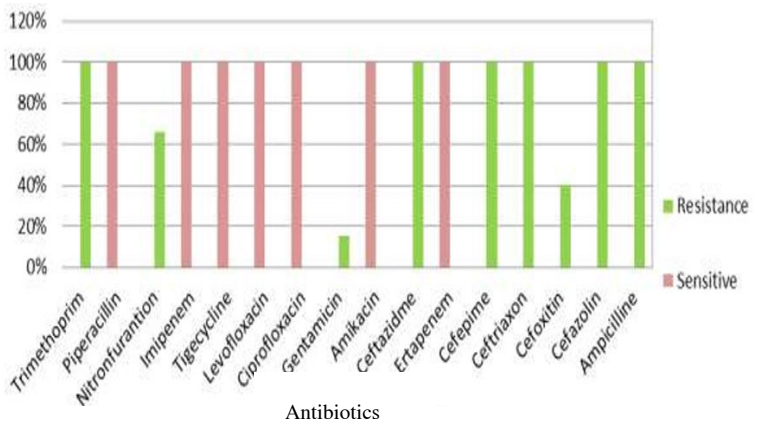

Figure 6: The Percentage of Antibiotic Susceptibility for *E. coli* Isolates in This Study

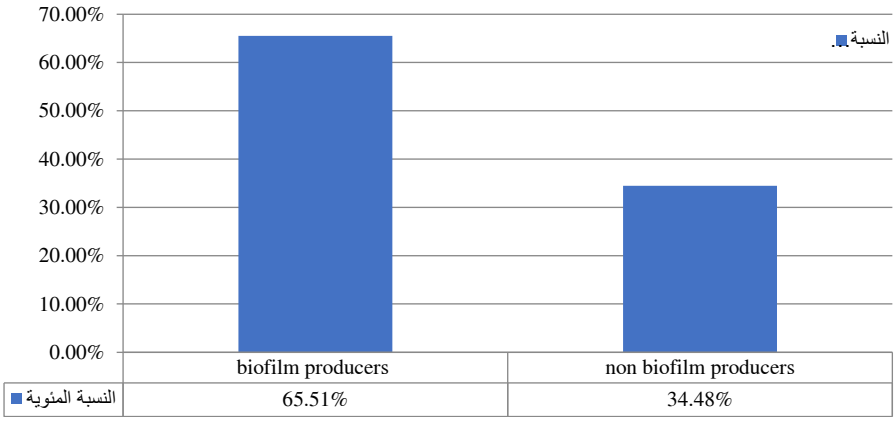

Figure 7: Prevalence of *E. coli* Isolates as Biofilm Producers by Microtiter Plate Method

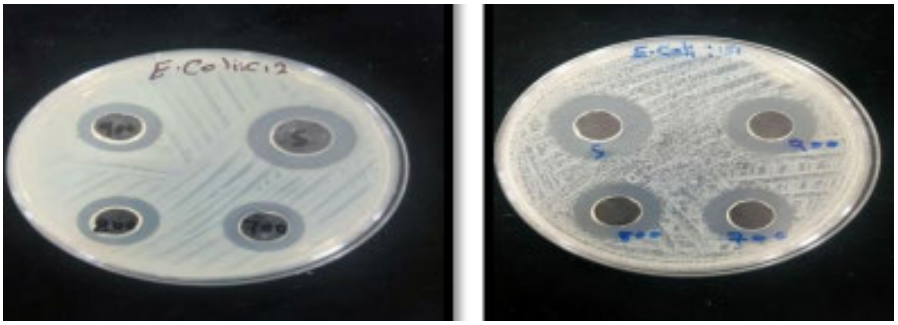

Figure 8: Antibacterial Activity of Mg Against Some Resistant *E. coli* on Muller-Hinton Agar

react with proteins by combining the thiol (SH) groups, which results in the inactivation of the proteins [27] (Figure 8).

Effect of Different Concentrations of Mg Nanoparticles on Biofilm Formation of Some MDR Antibiotic Isolates of *E. coli*

The findings demonstrated that the inhibition zone of biofilm formation for resistant *E. coli* isolates grew steadily as the concentration of magnesium nanoparticles rose, peaking at 400 µg/ml. Complex bacterial populations known as biofilms are immune system and drug resistant. Nanoparticles, a potentially significant candidate treatment, were utilised to demonstrate anti-biofilm activity in order to address the issue of the absence of effective antibiofilm antibiotics [24].

Without being exposed to the nanoparticles, the majority of the isolate's bacteria showed signs of being able to build biofilm; however, when *E. coli* was exposed to magnesium, this ability was inhibited and eliminated. When nanoparticles penetrate biofilms, they reduce the growth rate and expression of resistance genes [14]. This has an impact

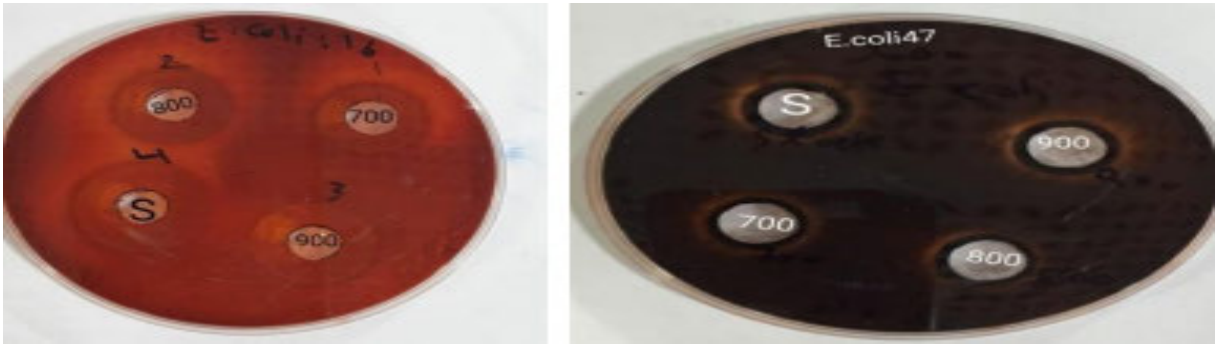

Figure 9: Antibiofilm Formation Against Some Resistant *E. coli*, 24h in 37°C, on Congo Red Agar. 0.01, 0.009, 0.008, 0.007 mg/ml

on the development of microcolonies and the maturation of biofilms. As a result, Mg may be utilised to prevent and cure illnesses linked to biofilms [25].

The structural differences in the cell wall composition of G+ve and G-ve bacteria may be the reason for the lower antibiofilm activity of magnesium against G+ve bacteria compared to G-ve bacteria [23]. Other research showed that magnesium has antibiofilm ability against both G+ve and G-ve bacteria, as evidenced by the nearly total prevention of biofilm formation by *E. coli* when Mg-coated catheters were tested *in vitro* [25]. The EPS matrix of the biofilm architecture may be jeopardised by generated hydroxyl radicals since they have the ability to depolymerise polysaccharides, damage DNA and deactivate enzymes [26]. These findings contrast with those of another investigation, which discovered that magnesium (mean diameter 50 nm) virtually totally inhibited *P. aeruginosa* and *S. biofilm* formation. epidermidis by preventing the first stage of bacterial surface attachment [23]. Nowadays, it is impossible to treat many illnesses with a single antibiotic; instead, a combination of antibiotics is needed. When the pathogen lives inside a biofilm or develops an intracellular lifestyle, therapy becomes more difficult. Effective treatment of these infections is hampered by the need to administer high doses of antibacterial medications, which is frequently challenging because of drug toxicity [23,26]. Consequently, there are four potential future routes for employing magnesium nanoparticles to address these issues (Figure 9).

CONCLUSIONS

In the fields of biomedicine and pharmaceuticals, the development of resistance against human infections is a challenge. Concern over the introduction and reemergence of MDR pathogens is a result of antibiotic resistance profiles. In the current period, improving the bactericidal capability of antimicrobial substances through development or modification is a priority. A good platform for creating and modifying nanostructures with potential uses in a variety of fields is provided by nanotechnology. Thus, it was discovered that certain antibiotics and magnesium nanoparticles were. These are effective weapons against MDR *E. coli*, which produces strong biofilms and they also boost the antibiotic's effectiveness.

REFERENCES

[1] Al-Taee, E.H. "Effect of Silver Nanoparticles Synthesized Using Leaves Extract of Olive on Histopathological and Cytogenetic Effects in Albino Mice." *Iraqi Journal of Agricultural Sciences*, vol. 51, no. 5, 2020, pp. 1448-1457.

[2] Aslam, B. *et al.* "Antibiotic Resistance: A Rundown of a Global Crisis." *Infection and Drug Resistance*, 2018, pp. 1645-1658.

[3] Atwan, Q.S. and N.H. Hayder. "Eco Friendly Synthesis of Silver Nanoparticles by Using Green Method: Improved Interaction and Application *In Vitro* and *In Vivo*." *Iraqi Journal of Agricultural Science*, vol. 1, Special Issue, 2020, pp. 201-216. https://doi.org/10.1134/S0020168507050111.

[4] Funari, R. and A.Q. Shen. "Detection and Characterization of Bacterial Biofilms and Biofilm-Based Sensors." *ACS Sensors*, vol. 7, no. 2, 2022, pp. 347-357.

[5] Ibrahim, O.M.S. *et al.* "Evaluation of Biological Activity of Greenly Synthesized Silver Nanoparticles Using Aloe Vera Gel Extract as Antibacterial Agent *In Vitro* and *In Vivo*." *Iraqi Journal of Agricultural Science*, vol. 51, no. 6, 2020, pp. 1706-1715.

[6] Kalishwaralal, K. *et al.* "Mg Nanoparticles Impede the Biofilm Formation by Pseudomonas aeruginosa and Staphylococcus epidermidis." *Colloids and Surfaces B: Biointerfaces*, vol. 79, 2020, pp. 340-344.

[7] Markowska, K. *et al.* "Mg Nanoparticles as an Alternative Strategy against Bacterial Biofilms." *Acta Biochemica Polonica*, vol. 6, no. 4, 2021, pp. 523-530.

[8] Mohamed, A.K.S. *et al.* "Interactive Effect of Salinity and Mg Nanoparticles on Photosynthetic and Biochemical Parameters of Wheat." *Archives of Agronomy and Soil Science*, vol. 63, no. 12, 2017, pp. 1736-1747.

[9] Nadia, G.K. *et al.* "Mg Nanoparticles: Effect on Antimicrobial and Antifungal Activity of New Heterocycles." *Bulletin of the Korean Chemical Society*, vol. 31, no. 12, 2019.

[10] Newell, D.G. and R.M. La Ragione. "Enterohaemorrhagic and Other Shiga Toxin-Producing *Escherichia coli* (STEC): Where Are We Now Regarding Diagnostics and Control Strategies?" *Transboundary and Emerging Diseases*, 2018.

[11] Le, N.A. "Lipoprotein-Associated Oxidative Stress: A New Twist to the Postprandial Hypothesis." *International Journal of Molecular Sciences*, vol. 16, no. 1, 2018, pp. 401-419.

[12] Nithya, G.N. *et al.* "Biosynthesis of Nanoparticle and Its Antibacterial Activity." *Archives of Applied Science Research*, vol. 3, 2022, pp. 377-380.

[13] Panda, P.S. *et al.* "Comparison of Four Different Methods for Detection of Biofilm Formation by Uropathogens." *Indian Journal of Pathology and Microbiology*, vol. 59, no. 2, 2016.

[14] Rahman, A.E. *et al.* "Managing Neonatal and Early Childhood Syndromic Sepsis in Resource-Poor Settings." *PLOS One*, vol. 12, 2017. https://doi.org/10.1371.

[15] Ruchi, T. *et al.* "Comparison of Phenotypic Methods for the Detection of Biofilm Production in Uropathogens in a Tertiary Care Hospital in India." *International Journal of Current Microbiology and Applied Sciences*, vol. 4, no. 9, 2023, pp. 840-849.

[16] Ukah, U.V. *et al.* "Risk Factors for Acquisition of Multidrug-Resistant Escherichia coli and Development of Community-Acquired Urinary Tract Infections." *Epidemiology and Infection*, vol. 146, no. 1, 2018, pp. 46-57.

[17] Rodríguez-Hernández, A.P. *et al.* "Antibacterial Properties In Vitro of Magnesium Oxide Nanoparticles for Dental Applications." *Nanomaterials*, vol. 13, 2023.

[18] Vanaja, M. and G. Annadurai. "Coleus aromaticus Leaf Extract Mediated Synthesis of Mg Nanoparticles and Its Bactericidal Activity." *Applied Nanoscience*, vol. 3, no. 1, 2019, pp. 217-223.

[19] Vincent, M.G. *et al.* "In Vitro Study on the Efficacy of Zinc Oxide and Titanium Dioxide Nanoparticles against Metallo Beta-Lactamase and Biofilm Producing Pseudomonas aeruginosa." *Journal of Applied Pharmaceutical Science*, vol. 4, no. 7, 2022, pp. 041-046.

[20] Xiu, Z.M. *et al.* "Differential Effect of Common Ligands and Molecular Oxygen on Antimicrobial Activity of Silver Nanoparticles versus Ions." *Environmental Science and Technology*, vol. 45, 2020, pp. 9003-9008.

[21] Girma, W.M. *et al.* "Biogenic Synthesis and Characterisation of MgO Nanoparticles Using Verbascum Sinaiticus." *Materials Advances*, vol. 6, 2025, pp. 4003-4015.

[22] Amrullah, H. *et al.* "Antioxidant and Antibacterial Activities of Magnesium Oxide Nanoparticles Prepared Using Aqueous Extract of Moringa Oleifera Bark." *Journal of Multidisciplinary Applied Natural Science*, vol. 1, 2021, pp. 44-53.

[23] Hassan, S.E.D. *et al.* "Rhizopus oryzae-Mediated Green Synthesis of Magnesium Oxide Nanoparticles (MgO-NPs)." *Journal of Fungi*, vol. 7, 2021.

[24] Saleh, M.N. and S. Khoman Alwan. "Bio-Synthesis of Silver Nanoparticles from Klebsiella pneumonia: Characterization and Antibacterial Studies." *Journal of Physics: Conference Series*, vol. 1664, 2020.

[25] Abdel-Maksoud, G. *et al.* "Green Synthesis of Magnesium Oxide Nanoparticles Using Lactobacillus gasseri." *Egyptian Journal of Chemistry*, vol. 66, 2023, pp. 179-189.

[26] Singh, A. *et al.* "Green Synthesis of Metallic Nanoparticles as Effective Alternatives to Treat Antibiotic Resistant Bacterial Infections." *Biotechnology Reports*, vol. 25, 2020.

[27] Bhardwaj, K. *et al.* "Conifer-Derived Metallic Nanoparticles: Green Synthesis and Biological Applications." *International Journal of Molecular Sciences*, vol. 21, 2020.

[28] Amrullah, H. *et al.* "Antioxidant and Antibacterial Activities of Magnesium Oxide Nanoparticles Prepared Using Aqueous Extract of Moringa Oleifera Bark." *Journal of Multidisciplinary Applied Natural Science*, vol. 1, 2021, pp. 44-53.

[29] Bhardwaj, K. *et al.* "Conifer-Derived Metallic Nanoparticles: Green Synthesis and Biological Applications." *International Journal of Molecular Sciences*, vol. 21, 2020.